Heavy rain analysis based on GNSS water vapour content in the Spanish Mediterranean area

E. Priego,[a]* A. Seco,[b] J. Jones[c] and M. J. Porres[a]
[a] *Universitat Politècnica de València, Spain*
[b] *Public University of Navarre, Pamplona, Spain*
[c] *Met Office, Exeter, UK*

ABSTRACT: For improved water resource management and forecasting of risks associated with hydrological processes, it is fundamental to improve the knowledge of rainfall as a natural process. Atmospheric water vapour content is one of the key variables in precipitation. The distribution and evolution of atmospheric water vapour is critical for the functioning of hydrological processes, being one of the essential climate variables as defined in the Global Climate Observing System. Improving understanding of atmospheric water vapour content and distribution is essential for climate change studies because water vapour is the main greenhouse gas, contributing around 70% of global temperature rise (Solomon *et al.,* 2007). Water vapour is also a major component in controlling atmospheric stability, because it is involved actively in the evolution and propagation of convective storm systems. Until recently, atmospheric water vapour could not be observed particularly well due to the absence of instruments capable of measuring it at high-resolution temporal and spatial scales. However, in recent years the increase in the number of permanent GNSS (Global Navigation Satellite System) reference stations worldwide has led to a major breakthrough in the monitoring of atmospheric integrated water vapour (IWV), with almost 2000 sites in Europe alone contributing near real-time atmospheric delay estimates. The present study focuses on the relationship between variations in IWV observed using delays in GNSS signals with meteorological variables such as atmospheric pressure and precipitation, in a long-term study for the period 2000 – 2012 in the area of Valencia, Spain. Fluctuations in IWV fields correlate well with approaching frontal rainfall, and a combined rise in IWV and fall in atmospheric pressure act together as a precursor to heavy precipitation.

KEY WORDS integrated water vapour (IWV); Global Navigation Satellite Systems (GNSS); precipitation; meteorology; remote sensing; climate trends and variability

1. Introduction

The water on planet Earth appears naturally in all three physi- cal states: gas (water vapour) in the atmosphere, solid ice and snow, and as liquid water in oceans, rivers, lakes and aquifers. Most (97.2%) water is saline with the remainder being fresh, distributed as groundwater (2.8%), glaciers and ice caps (2.1%), lakes and rivers (0.02%) and soil moisture (0.005%); atmospheric water vapour constitutes only *ca* 0.001% of the total (Raghunath, 2006).

Atmospheric water vapour has a complex life cycle, which includes vertical and horizontal transport, mixing, condensation, precipitation and evapotranspiration. The content of water vapour is an indicator of the moisture conditions in the troposphere, and is an indicator of the volume of water which could (theoretically) result from precipitation in unstable conditions. Water vapour is currently undersampled in typical meteorological and climate observing systems; therefore, obtaining and exploiting additional high-quality humidity observations is essential to the advancement of climate monitoring (Guerova *et al.,* 2013).

Global Navigation Satellite System (GNSS) technology can deliver an accurate estimate of atmospheric integrated water vapour (IWV), due to the effect of the neutral atmosphere on the signal propagation (mapped to zenith angle) and the values of mean atmospheric temperature and ground air pressure (Bevis *et al.,* 1992). Thanks to permanent GNSS stations worldwide, atmospheric water vapour can be estimated continuously, improving forecast skill in the distribution and extent of humidity fields. GNSS technology has demonstrated its capacity as an accurate sensor of atmospheric water vapour for some time, with operational assimilation under way at a number of European national meteorological institutes (Guerova *et al.,* 2003, 2005; Morland and Mätzler, 2007; Morland *et al.,* 2009). However, monitoring intense precipitation associated with convection has only been demonstrated more recently (Graham *et al.,* 2012; Seco *et al.,* 2012; de Haan, 2013). Several studies have established the existence of high water vapour content in the atmosphere before intense precipitation occurrences in the Mediterranean area (Champollion *et al.,* 2004; Cucurull *et al.,* 2004; Brenot *et al.,* 2006).

The present case study is an experimental analysis of the spatial and temporal variability of IWV associated with the onset of heavy precipitation in a region of eastern Spain. In this region, it is difficult to forecast precipitation due to high temporal and spatial variability, even on a sub-daily and hourly basis. This region has recorded some of the highest values in Europe for daily concentration of precipitation (the top 25% of wet days contribute to 75% of the annual total rainfall).

Figure 1. Location of study area in Spain. ALAC, Alicante; ALCO, Alcoi; AYOR, Ayora; BORR, Burriana; DENI, Denia; MALL, Mallorca; MORE, Morella; MURC, Murcia; TORR, Torrevieja; UTIE, Utiel; VALE, Valencia; VCIA, Valencia; ZARA, Zaragoza.

2. Materials and methods

2.1. GNSS and meteorological data

GNSS IWV estimates were obtained from 13 sites from the Valencia region of Spain (Figure 1). Four stations [Alicante (ALAC), Mallorca (MALL), Valencia (VALE) and Zaragoza (ZARA)] belong to the National Geographical Institute, eight [Alcoi (ALCO), Ayora (AYOR), Burriana (BORR), Denia (DENI), Morella (MORE), Torrevieja (TORR), Utiel (UTIE) and Valencia (VCIA)] belong to the ERVA network of the Valencia Cartographic Institute and the station in Murcia (MURC) belongs to the Meristemun network. For the case studies in Sections 3.3 and 3.4, data from GNSS stations ALAC and VALE were used, because they have the longest available time series of data (2000 – 2012).

Meteorological data, atmospheric pressure and observations of precipitation were supplied by the Spanish Meteorology Agency (AEMET). The meteorological observing stations are distributed throughout the study area and collocated with the GNSS stations, with precipitation observations available at an hourly frequency.

In addition, three GNSS sites situated very close to three radiosounding stations (type RS92SGP) were used to verify the GNSS IWV estimates. Radiosonde integrated precipitable water vapour (RS IWV) observations have a 12 h interval with observations at 0000 UTC and 1200UTC. Radiosonde data were available for the period 2006 – 2011 at Zaragoza and Murcia and 2001 – 2011 at Mallorca.

2.2. Estimation of GNSS IWV

The effect of the troposphere causes delays in GNSS signal propagation, which must be estimated in high-precision geodetic applications. The delays to each satellite are mapped to the vertical and this parameter is known as zenith total delay (ZTD) (i.e. the total signal delay due to the neutral atmosphere at zenith).

The ZTD can be separated further into a hydrostatic component (zenith hydrostatic delay or ZHD) caused by all atmospheric components and a nonhydrostatic or 'wet' delay (zenith wet delay, ZWD), caused primarily by atmospheric water vapour.

$$ZTD = ZHD + ZWD \quad (1)$$

$$ZHD = 10^{-6} \int N_{hydro}\, dz \quad (2)$$

$$N_{hudro} = K_1 \frac{P}{T_V} \quad (3)$$

where TV is the virtual temperature.

$$ZWD = 10^{-6} \int N_{wet}\, dz \quad (4)$$

$$N_{wet} = K'_2 \frac{P_W}{T} + K_3 \frac{P_W}{T^2} \quad (5)$$

N_{wet} is due to the specific contribution of the dipole moment of water vapour molecules at the frecuency of the GNSS signal.

Of interest in meteorology and climatology is the accurate estimation of ZWD, which is a measure of the total amount of water vapour in the atmospheric column above a GNSS receiver. ZHD is relatively stable and it is directly proportional to the ground atmospheric pressure. It can be determined with an accuracy that is better than 1% using the Saastamoinen model (Saastamoinen, 1972):

$$ZHD = \frac{K_1 R_d P_a}{9.784(1-0.0026\cos(2\phi)-2.8\times10^{-7}H_a)} \times 10^{-3}(mm) \quad (6)$$

Where K_1 is 77.6 K h Pa^{-1} (Bevis *et al.*, 1994), R_d is the specific gas constant for dry air (287.0586 J kg K^{-1}), ϕ is the latitude

in degrees and H_a is the surface height above the ellipsoid in kilometres.

ZWD is responsible for the majority of short-term variation in ZTD due to the heterogeneity of the water vapour content in the atmosphere. In the present study, ZTD values were processed using the GAMIT GNSS processing software, setting the value of ZTD as a stochastic variation of the Saastamoinen model with piecewise linear interpolation of the data within the processing epoch (Herring *et al.*, 2006). The first calculation provides precise co-ordinates for the local stations for each 24 h of measurements, where tropospheric parameters have been estimated with a 2 h resolution (Brenot *et al.*, 2006). The final positions of the stations in the ITRF2000 reference frame (Altamimi *et al.*, 2002) were obtained as part of a global solution using the Kalman filter (Herring *et al.*, 2006). Subsequent zenith delays were calculated hourly. Baselines greater than 2000 km were used in order to decorrelate the tropospheric parameters from vertical posi- tion estimations (Tregoning *et al.*, 1998). The GNSS stations that were used were Brussels (BRUS), Cagliari (CAGL) and United States Naval Observatory (USNO). The Global Mapping Func- tion (GMF) was used to map the slants to the zenith and raw RINEX format data were used with a sampling rate of 30 s and an elevation cut-off angle of 10° (Pacione *et al.*, 2001). The variations were constrained using a Gauss–Markov process with an *a priori* power density.

ZTD measurements were produced using a sliding window strategy with sessions of 25 h shifted by 12 h. The system uses two 25 h sliding windows for each day to obtain hourly ZTD values, removing the first six and last seven values from each sliding window. The system uses only the 12 central values from each window, to avoid the edge effect of the Gauss–Markov process (Jin *et al.*, 2007).

Furthermore, if the weighted mean atmospheric temperature (T_m) is calculated then ZWD can be converted easily to IWV, according to Bevis *et al.* (1994):

$$IWV = \frac{10^{-6}}{R_w(K'_2 + \frac{K_3}{T_m})} ZWD \qquad (7)$$

where R_w is the specific gas constant of water vapour (461.495 J kg^{-1} K^{-1}), $K'_2 = 70.4 \pm 2.2$ K hPa^{-1} (Bevis *et al.*, 1994) and $K_3 = 3.739 \pm 0.012\ 10^5$ K hPa^{-1} (Bevis *et al.*, 1994).

3. Results and discussion

3.1. GNSS IWV and RS IWV analysis

In order to perform a processing strategy verification check, three radiosonde time series (RS IWV) were compared against GNSS (GNSS IWV) estimates at Zaragoza and Murcia, for a period of 6 years between 2006 and 2011, and at the station in Mallorca, for a period of 11 years between 2001 and 2011.

Figure 2 shows the correlation between the GNSS IWV and RS IWV values, where $R^2 = 0.87$ and the Pearson corre- lation coefficient (PCC) = 0.93 for Zaragoza, $R^2 = 0.89$ and PCC = 0.94 for Murcia, and $R^2 = 0.89$ and PCC = 0.95 for Mallorca were obtained. These results demonstrate the quality of the GNSS processing strategy and the capacity of the GNSS to measure atmospheric water vapour content accurately (Seco *et al.*, 2012).

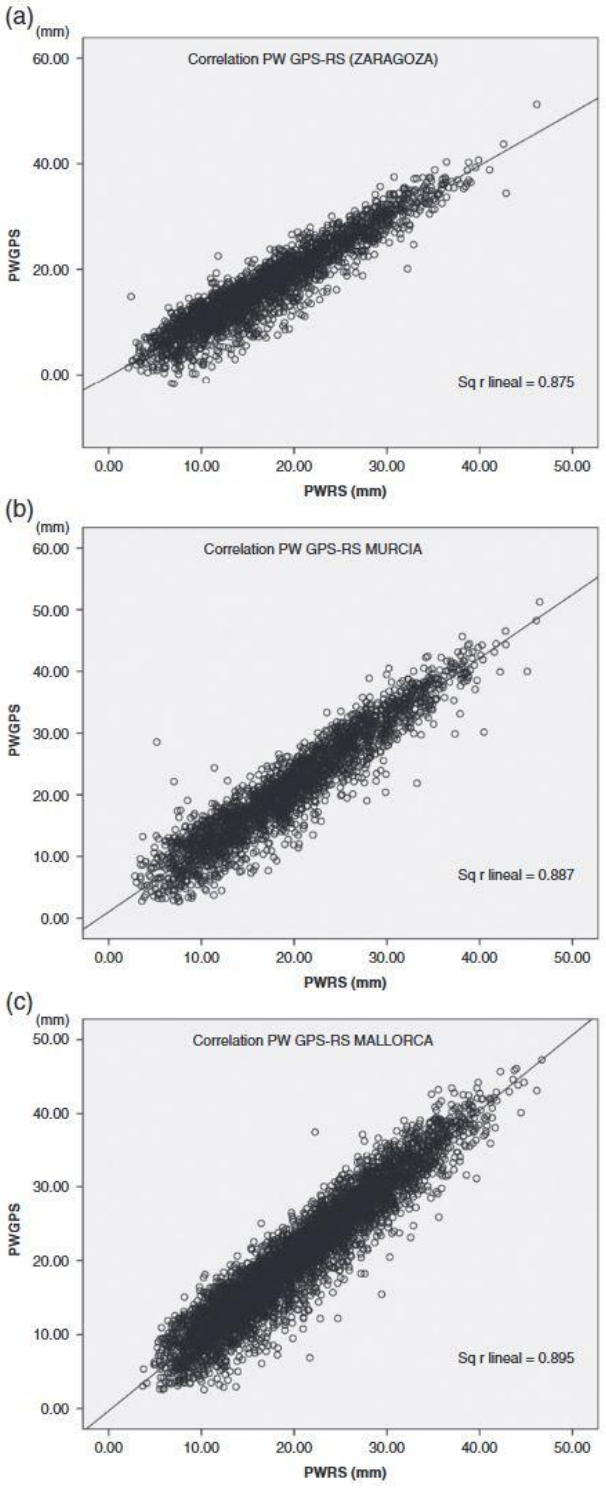

Figure 2. Comparison of radiosounding system and Global Navigation Satellite System integrated water vapour (GNSS IWV) values for Zaragoza (a), Murcia (b) and Mallorca, Spain (c). PWRS, precipitable water obtained with radiosonde; PWGPS, precipitable water obtained with GPS.

3.2. Time series GNSS IWV

The study of the climate system is, to a large extent, the study of the statistics of weather (Zwiers and Von Storch, 2004). For climate applications, time series of IWV longer than a few decades are required (Gradinarsky *et al.*, 2002). The Global Cli- mate Observing System states that any climatological reference period must be 30 years; GNSS networks now have a temporal coverage of 15 – 20 years and for this reason GNSS IWV cannot yet be used as a climatological reference.

As well as identifying trends, it is also possible to identify atmospheric variability (diurnal, seasonal and annual cycles) and

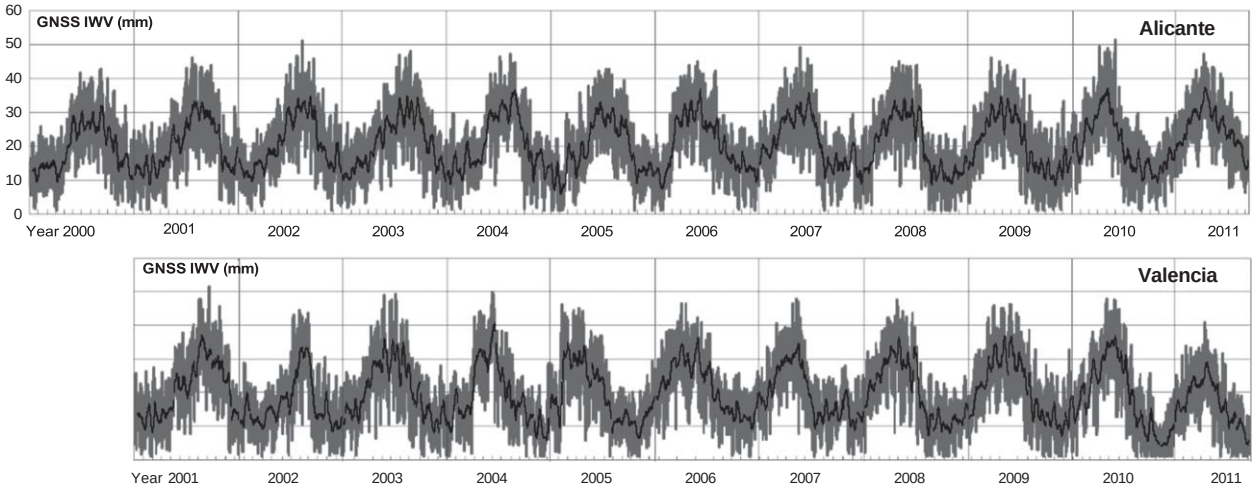

Figure 3. Homogeneous integrated water vapour (IWV) time series for Alicante (2000–2011) and Valencia, Spain (2001–2011).

uncertainty estimates. Figure 3 shows the evolution of IWV for the GNSS stations at Alicante (ALAC) and Valencia (VALE) for an 11 year period, from 2001 and 2011. A clear annual cyclical signal can be seen in the data obtained from several Spanish GNSS stations, where minimum values are obtained in the winter months and maximum values occur in summer, as expected (Bennouna *et al.*, 2013).

Alicante and Valencia are regions which exhibit some of the highest values of IWV in Europe due to the contribution of large amounts of moisture from the Mediterranean Sea (Vedel *et al.*, 2004; Riesco *et al.*, 2013). It was observed that the water vapour increased steadily from February to July, but decreased more sharply from summer to winter. This behaviour illustrates the local hydrological cycle in which the atmosphere is slowly loading water vapour (evaporation) during spring, which is discharged as precipitation in autumn and winter.

3.3. Identification of a potential IWV–pressure–precipitation relationship

The case study in the present paper examines the perceived relationship between precipitation and water vapour. The relationship was assessed using an IWV time series from GNSS against atmospheric pressure (P_{atm}) for a period of 11 years (2001 – 2011) for the VALE GNSS station at Valencia. The scatter plots in Figure 4 show the monthly relationship of IWV with P_{atm}. The light gray background data illustrate the total annual distribution of IWV/$P_{atm,}$ the dark gray data represent the monthly data and the black plots identify the combinations of values IWV/P_{atm} that caused rainfall (rainfall occurred only under certain conditions of IWV/P_{atm}). The circles indicate where the rainfall was >50% of the monthly total. The centre of the circle is defined by the average IWV/P_{atm} co-ordinates of the black plots. The radius of the circle shows the percentage of precipitation contained within it. In this case, it shows a rate of 50%, so the content inside the circle is half the volume of precipitation produced in the corresponding month.

It can be seen by comparison of the monthly spread *versus* the annual spread that the relationship of IWV/P_{atm} does change throughout the year ,with data for each month distributed predominantly in specific zones. In winter, the data are concentrated near the *y*-axis, in spring and autumn the data are more evenly spread in a circular fashion with a smaller spread, whereas in the summer months the data are in closer alignment to the *x*-axis. It can be seen that the mean spread moves along the *x*-axis to higher IWV values in summer and lower values in winter, as would be expected. It may also be noted that the precipitation data are concentrated in specific zones of the IWV/P_{atm} data for each month, typically on the high IWV boundary.

During the winter months (December, January and February), the scatter plot is narrower and more elongated along the *y*-axis, indicating that during this period the amount of atmospheric water vapour was low and relatively stable, whereas the atmo- spheric pressure was much more variable, ranging from 980 to 1030 hPa.

In March, coinciding with the beginning of spring, the scatter plot begins to move slightly to the right of the graph and has a smaller spread, with pressure values ranging from 990 to 1020 hPa. This trend is accentuated in April and May with all combinations of IWV/P_{atm} clustered in the centre of the graph in a more evenly circular distribution. Therefore, it seems that IWV values gradually increase and pressure begins to vary less in spring.

In June, the beginning of summer in the region, the centre of the scatter plot continues to move toward the area of higher IWV with lower *y*-axis spread indicating more barotropic conditions. During the months of July, August and September, the scatter plot adopts an elongated shape along the *x*-axis, with peak IWV values of up to ∼50 mm and very stable atmospheric conditions, with P_{atm} values ranging from 1000 to 1015 hPa. In September, the scatter plot follows the same pattern as that of the summer months but increases slightly in size, indicating greater baroclinic conditions.

During autumn, an especially atmospherically baroclinic season, the data begin to disperse and to move towards the *y*-axis with lower IWV values. Finally, the spread for November and December returns to the specific distribution of winter, but with greater IWV spread than for January and February.

These charts use GNSS IWV in combination with atmospheric pressure observations to illustrate the range and variability in atmospheric conditions in Valencia. If precipitation data are added to the plots, it can be seen that at a fixed pressure level rainfall generally occurred at the highest value of IWV. It is worth noting that these circles are predominantly located just below the average P_{atm} for the month and where values of IWV are high (in relation to the P_{atm}), indicating that where there is lower P_{atm}

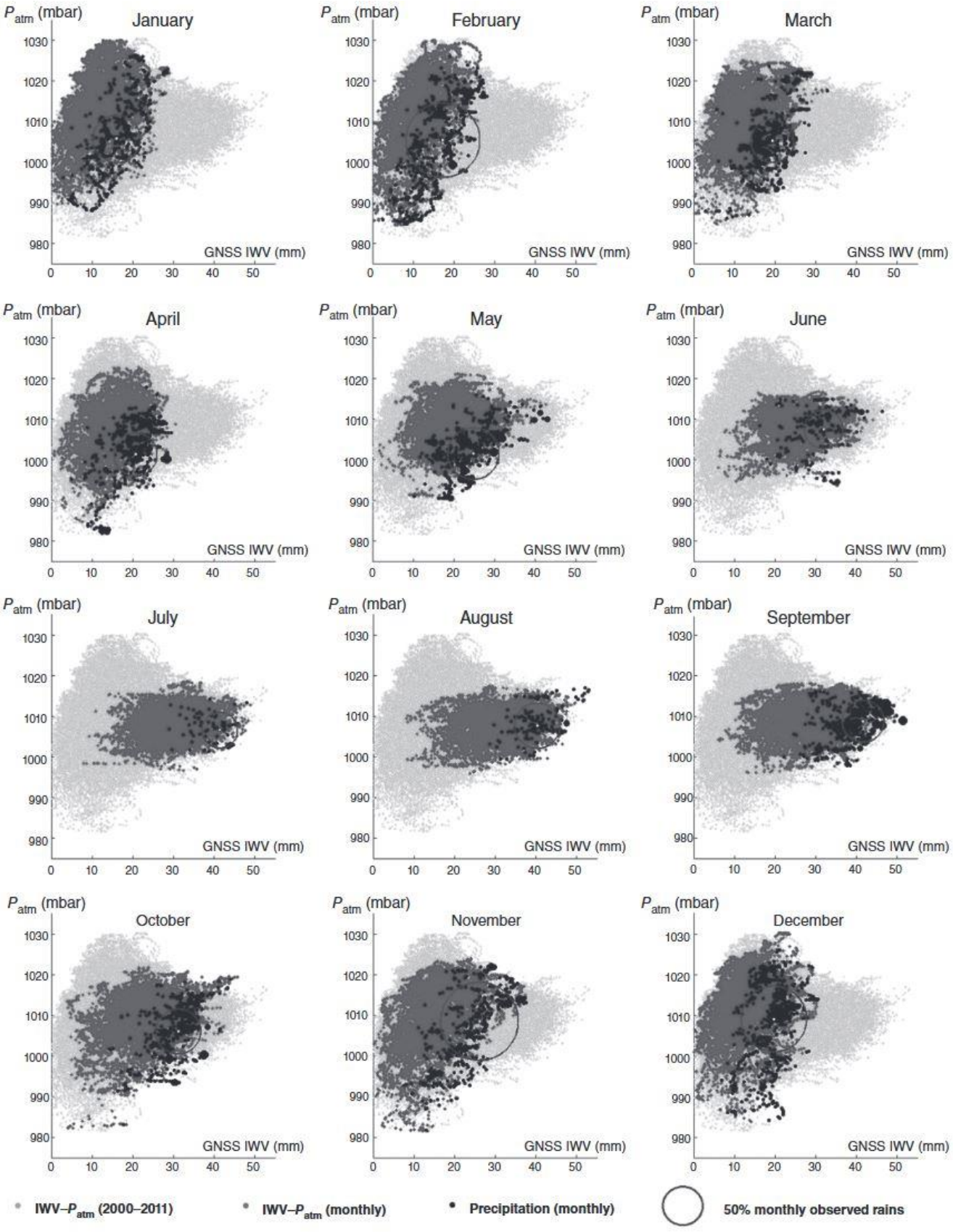

Figure 4. Monthly Global Navigation Satellite System integrated water vapour (GNSS IWV) *versus* atmospheric pressure (P_{atm}) plots (dark gray data) for Valencia, Spain (2000–2011). The light gray background indicates the annual total and data for when precipitation occurred are indicated in black. Circles indicate 50% monthly observed rain.

Table 1. Episodes of heavy rain (2001–2011, Valencia, Spain).

Date	Accumulated rainfall (mm)	Duration (h)	Δ(IWV) before	Δ(P_{atm}) before	Δ(IWV) after	Δ(P_{atm}) after
5 September 2001	32.3	1	+14	−12	−12	0
6 September 2001	14.5	1	+4	−14	−6	+8
9 October 2001	18.9	1	+9	−4	−4	+28
2 September 2002	56.1	2	+8	+1	−8	+4
6 September 2003	24.8	2	+2	−20	−10	−6
2 September 2004	92.2	3	+9	+26	−6	+8
3 September 2004	46.6	1	+6	−4	−6	+33
21 October 2004	19.6	1	+4	−13	−2	+23
17 September 2005	15.2	1	+3	+12	−5	+20
18 October 2006	29.4	1	−4	−14	−5	−2
14 September 2007	54.3	6	+7	+20	−6	+27
21 September 2007	49.0	4	+8	−13	−9	−7
12 October 2007	178.2	11	+11	−4	−10	+26
17 September 2010	30.2	1	+8	+44	−10	+11
9 October 2010	20.8	1	+6	−18	−16	−42
12 October 2010	17.9	1	+8	−10	−5	+20
23 September 2011	29.5	1	+13	−3	−9	−4
21 October 2011	19.6	1	+5	−1	−3	+11

Setting for three parameters: time window; IWV, integrated water vapour; P_{atm}, atmospheric pressure.

and relatively high IWV, heavy rainfall may occur. It is worth noting also that precipitation occurs across a wide range of P_{atm} levels, but only where IWV is high, indicating that rainfall is highly correlated with atmospheric water vapour content and less so to atmospheric pressure, at least in the area of study. Maximum rainfall intensity occurs in September and October, when the values of IWV are higher, not when P_{atm} values are lowest.

3.4. Severe rainfall events

The two main characteristics that define rainfall in the region are (1) its variability (Haase *et al.*, 2003) and (2) episodes of severe rainfall.

In the present analysis, rainfall in the city of Valencia in the study period (2001 – 2011) was evaluated. The average annual precipitation in Valencia is 420 mm, and the majority of the rainfall occurs in September and October. During the study period, there were 18 episodes registered (Table 1) (11 cases in September and seven in October) that the AEMET classified as heavy rainfall.

Figures 5(a) and (b) show the time evolution of IWV in mm (line) and atmospheric pressure in hectopascals (line) along with the amount of rainfall (bar) registered in each rainy episode, where the accumulated rainfall data are hourly values (mm). The horizontal axis defines the time interval (hourly). The left vertical axis indicates the amount in mm of rain and IWV. The right vertical axis indicates the atmospheric pressure in hPa.

A preliminary warning system was considered for this study (Table 1, Figures 5(a) and (b)). A setting for three parameters was used. The first parameter is the time window before and after the highest rain accumulation of an event. In this case, a 6 h time window was chosen. The second parameter is the rise of IWV during the time window, and the third parameter the rise or fall of pressure. All cases show a clear increase in IWV, a few hours before the onset of precipitation. In addition, the maximum value of IWV occurs almost simultaneously with the peak intensity of rain.

According to Table 1, in all cases except one, IWV increased in the range of 2 – 14 mm, 6 h before precipitation, with an average rise of 7.4 mm. A further decrease was seen of between 2 and 16 mm after the rainfall, with an average drop of 7.4 mm. The results show that, before the storm occurs, there is an up to 25% average increase in IWV values at GNSS stations.

However, the behaviour of atmospheric pressure shows a great deal of variability and many torrential rainfall events have occurred accompanied by higher than typical atmospheric pressure levels. Thus, the key element in this type of rainfall is the atmospheric water vapour, acting as a 'rainfall release factor'. This indicator operates in the same way for all examples in this study.

The most severe rainfall occurred on 11 – 12 October 2007, causing a great deal of flooding and disruption to the region around Valencia (Figure 6). Rainfall data are hourly accumulated values in mm (bar), with an accumulated total of 178 mm being recorded within a 14 h period. That day the maximum intensity of the whole period was registered, with 47 mm in 1 h.

It can be observed from Figure 6 that prior to the episode of severe rainfall, there was an increase in IWV coupled with a decrease in pressure. A few hours prior to the start of the rain, IWV was stable with values typically *ca* 25 kg m^{-2}. Subsequently, a quick rise in IWV occurs, leading to the onset of the rain. The Mediterranean Sea, still warm in October, is a source of moisture content that continually recharges the atmospheric water vapour.

Other studies indicate that there is a strong spatial and temporal correlation between the variations of IWV and the passage of a storm (Choy *et al.*, 2013) and rainfall occurs mostly during high values of IWV (Guoping and Deng, 2013). An increase in IWV alone does not define when precipitation will occur; however, an increase in IWV followed by a sharp decrease in atmospheric pressure does seem to correlate with heavy precipitation. More study is required in this area to identify the correlation categorically, but potentially it is the basis for a future severe weather warning system.

4. Conclusions

Water vapour is a key ingredient of the global hydrological cycle and plays an important role in many atmospheric processes contributing to the weather and climate. The advantage of using ground-based Global Navigation Satellite System atmospheric

(a)

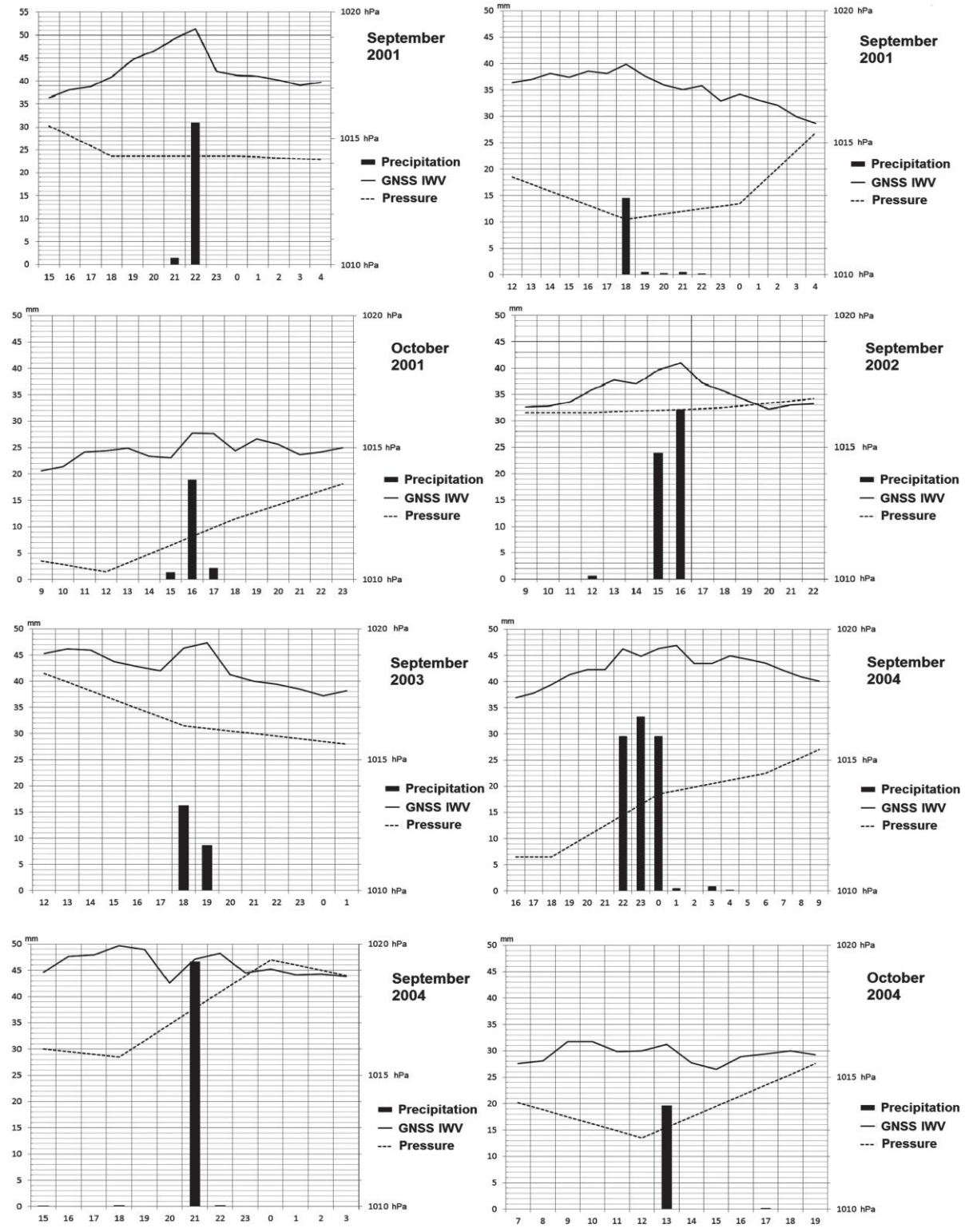

Figure 5. Heavy rainfall in Valencia, Spain (a) 2001 – 2004 and (b) 2005 – 2011

(b)

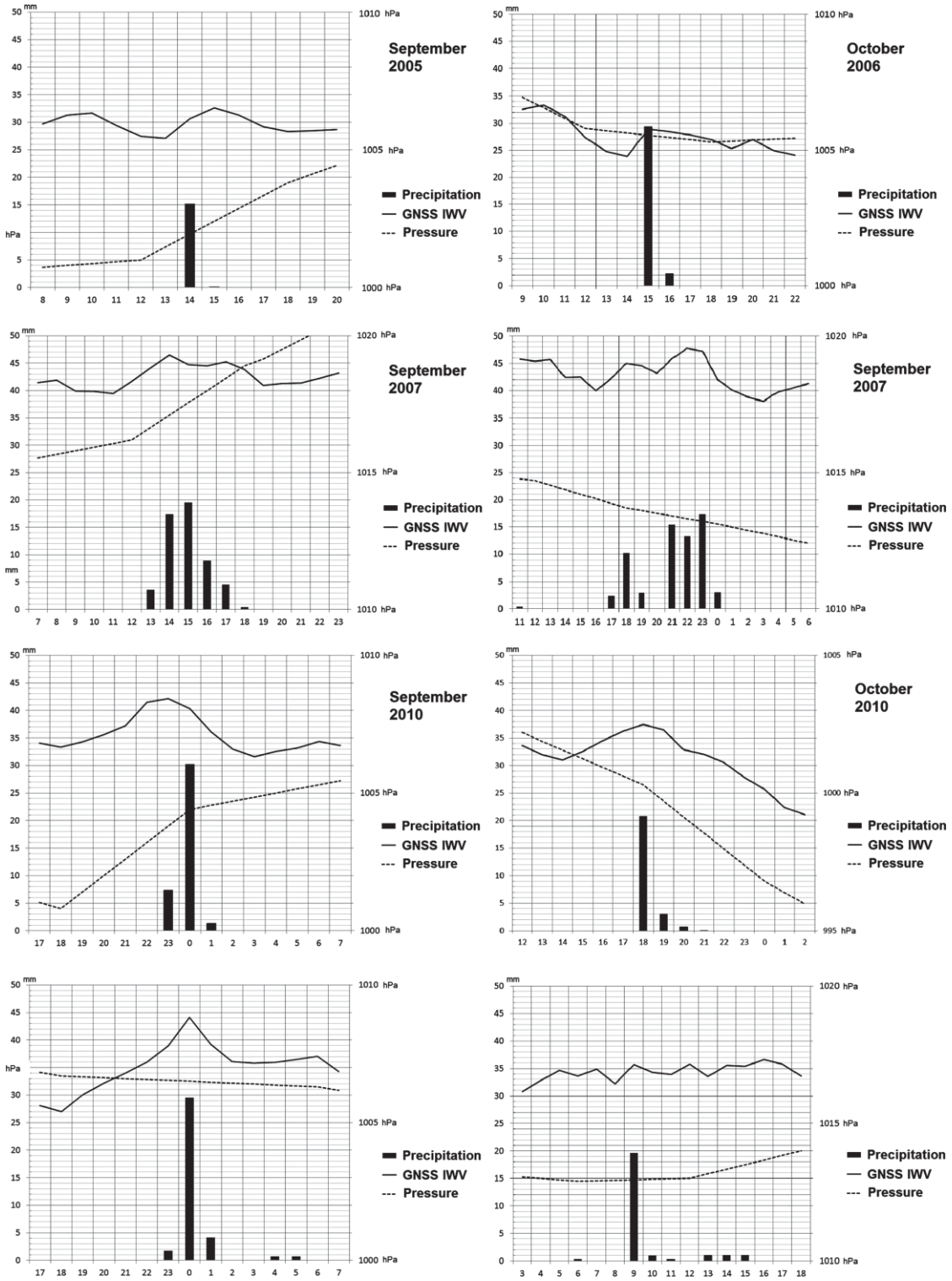

Figure 5. Continued.

integrated water vapour (GNSS IWV) is that it is capable of providing continuous observations with high temporal resolu- tion over a large geographical area. The existence for nearly 20 years of homogeneous observations from permanent GNSS stations worldwide has high potential for monitoring trends and variability in atmospheric water vapour, both on short timescales for severe weather and also for climate trend identification and characterization.

The graphical representation of the combination of variables IWV/P_{atm} (atmospheric pressure) provides a unique cluster of points for this climatic region (Figure 4). The rainfall events occur only on the right side of the graph, in the area of the highest

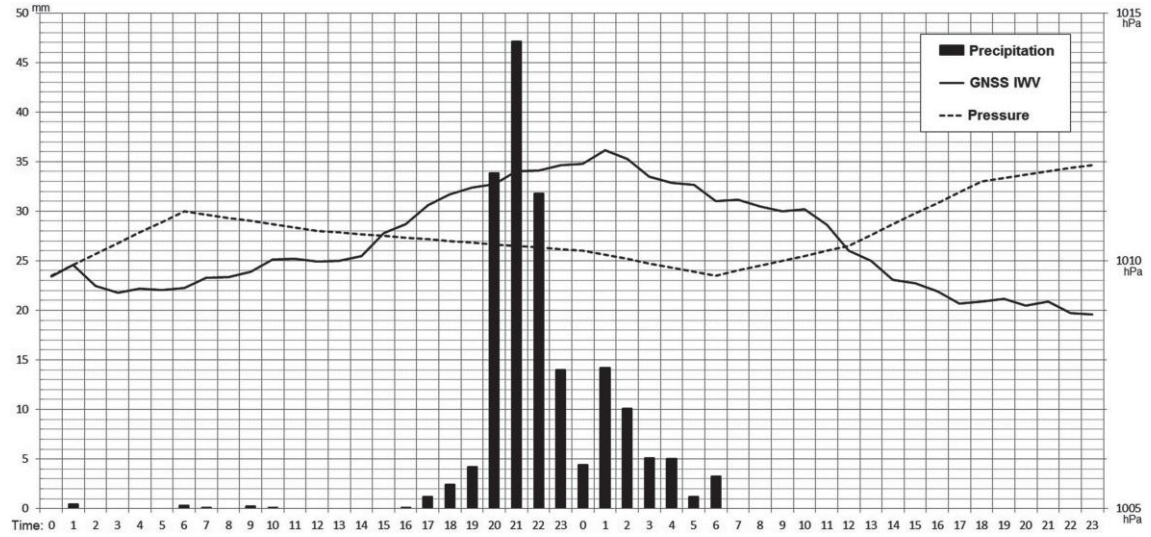

Figure 6. Time evolution of integrated water vapour (IWV) and atmospheric pressure along with the amount of rainfall registered in Valencia, Spain, 11 – 12 October, 2007.

values of IWV, which shows that the rainfall is highly related to the content of atmospheric water vapour.

In winter, there is a greater dispersion of rainfall cases regarding the relationship with IWV/P_{atm} compared to spring and summer, when rainfall occurs in a more concentrated form, reaching the maximum grouping in early autumn. Maximum intensity rainfall occurs in September and October when IWV values are at their highest. Changes in the positions of the centres of the circles move from a minimum value of 15.97 mm in January to a maximum value of 41.56 mm in September, in relation to the IWV co-ordinate. Pressure co-ordinates are irregular: they are positioned at the minimum co-ordinate (1001.23 hPa) in April and at the maximum co-ordinate (1009.18 hPa) in December.

There is a strong spatial and temporal correlation between the variations of IWV and the passage of a storm and rainfall occurred mostly during high values of IWV. The results show that large transfers of air and water vapour occur from the Mediterranean Sea to the coast, with an up to 25% increase in IWV values at GNSS stations. Heavy rain is associated with a continuous accumulation of IWV, which is the key element in severe rainfall events in the area of study.

References

Altamimi Z, Sillard P, Boucher C. 2002. ITRF 2000: a new release of the International Terrestrial Reference Frame for earth science applications. *J. Geophys. Res.* **107**: 2214.

Bennouna YS, Torres B, Cachorro VE, Ortiz JP, Toledano C, Berjón A, *et al*. 2013. The annual cycle of total precipitable water vapour derived from different remote sensing techniques: an application to several sites of the Iberian Peninsula. *Radiat. Processes Atmos. Ocean* **1531**: 296 – 299.

Bevis M, Businger S, Chiswell S, Herring TA, Anthes R, Rocken C, *et al*. 1994. GPS meteorology: mapping zenith wet delays onto precipitable water. *J. Appl. Meteorol.* **33**: 379 – 386.

Bevis M, Businger S, Herring TA, Rocken C, Anthes R, Ware R. 1992. GPS meteorology: remote sensing of atmospheric water vapour using the Global Positioning System. *J. Geophys. Res.* **97**(D14): 15787 – 15801.

Brenot H, Ducrocq V, Walpersdorf A, Champollion C, Caumont O. 2006. GPS zenith delay sensitivity evaluated from high-resolution numerical weather prediction simulations of the 8 – 9 September 2002 flash flood over southeastern France. *J. Geophys. Res.* **111**: D15105.

Champollion C, Masson F, Van Baelen J, Walpersdorf A, Chéry J. 2004. GPS monitoring of the tropospheric water vapour distribution and variation during the 9 September 2002 torrential precipitation episode in the Cévennes (southern France). *J. Geophys. Res.* **109**: D24102.

Choy S, Wang C, Zhang K, Kuleshov Y. 2013. GPS sensing of precipitable water vapour during the March 2010 Melbourne storm. *Adv. Space Res.* **52**: 1688 – 1699.

Cucurull L, Vanderberghe F, Barker D, Vilaclara E, Rius A. 2004. Three dimensional variational data assimilation of ground-based GPS ZTD and meteorological observations during the 14 December 2001 storm event over the western Mediterranean Sea. *Mon. Weather Rev.* **132**: 749 – e763.

de Haan S. 2013. Assimilation of GNSS ZTD and radar velocity for the benefit of very-short-range regional weather forecast. *Q. J. R. Meteorol. Soc.* **677**: 2097 – 2107.

Gradinarsky LP, Johansson JM, Bouma HR, Scherneck HG, Elgered G. 2002. Climate monitoring using GPS. *Phys. Chem. Earth* **27**: 335 – 340.

Graham E, Koffi EN, Maetzler C. 2012. An observational study of air and water vapour convergence over the Bernese Alps, Switzerland, during summertime and the development of isolated thunderstorms. *Meteorol. Z.* **21**: 561 – 574.

Guerova G, Brockmann E, Quiby J, Schubiger F, Matzler C. 2003. Validation of NWP mesoscale models with Swiss GPS Network AGNES. *J. Appl. Meteorol.* **42**: 141 – 150.

Guerova G, Brockmann E, Schubiger F, Morland J, Mätzler C. 2005. An integrated assessment of measured and modeled integrated water vapour in Switzerland for the period 2001 – 2003. *J. Appl. Meteorol.* **44**: 1033 – 1044.

Guerova G, Jones J, Dousa J, Dick G, De Haan S, Pottiaux E, *et al*. 2013. Advanced GNSS tropospheric products for monitoring severe weather. *Proceedings of the 4th International Colloquium Scientific and Fundamental Aspects of the Galileo Programme*, 4 – 6 December 2013, Prague, Czech Republic.

Guoping L, Deng L. 2013. Atmospheric water monitoring by using ground-based GPS during heavy rains produced by TIWV and SWV. *Adv. Meteorol.* **2013** article ID: 793957.

Haase J, Ge M, Vedel H, Calais E. 2003. Accuracy and variability of GPS tropospheric delay measurements of water vapour in the western Mediterranean. *J. Appl. Meteorol.* **42**: 1547 – 1568.

Herring T, King R, McClusky S. 2006. *GAMIT Reference Manual*. Department of Earth, Atmospheric, and Planetary Sciences, Massachusetts Institute of Technology.

Jin S, Park JU, Cho JH, Park PH. 2007. Seasonal variability of GPS-derived zenith tropospheric delay and climate implications. *J. Geophys. Res.* **112**: D09110.

Morland J, Collaud M, Hocke K, Jeannet P, Mätzler C. 2009. Tropospheric water vapour above Switzerland over the last 12 years. *Atmos. Chem. Phys.* **9**: 5975 – 5988.

Morland J, Mätzler C. 2007. Spatial interpolation of GPS integrated water vapour measurements made in the Swiss Alps. *Meteorol. Appl.* **14**: 15–26.

Pacione R, Sciarretta C, Vespe F, Faccani C, Ferretti R, Fionda E, *et al*. 2001. GPS meteorology: validation and comparisons with ground-based microwave radiometer and mesoscale model for the Ital- ian GPS Permanent Stations. *Phys. Chem. Earth* **26**: 139–145.

Raghunath HM. 2006. *Hydrology: Principles, Analysis and Design*. New Age International: New Delhi. ISBN: 978-81-224-3618-1.

Riesco J, Mora M, De Pablo F, Rivas L. 2013. Regimes of intense precipitation in the Spanish Mediterranean area. *Atmos. Res.* **137**: 66–79.

Saastamoinen J. 1972. Atmospheric correction for the troposphere and stratosphere in radio ranging of satellites. In *The Use of Artificial Satellites for Geodesy*, Geophysical Monograph Series, Hendriksen SW, Mancini A, Chovitz BH (eds), Vol. 15. American Geophysical Union: Washington, DC; 245–251.

Seco A, Ramírez F, Serna E, Prieto E, García R, Moreno A, *et al*. 2012. Rain pattern analysis and forecast model based on GPS estimated atmospheric water vapour content. *Atmos. Environ.* **49**: 85–93.

Solomon S, Qin D, Manning M, Chen Z, Marquis M, Averyt KB, *et al*. (eds). 2007. Climate change 2007: the physical science basis. In *Contribution of Working Group I to the Fourth Assessment Report of the Intergovernmental Panel on Climate Change*. Cambridge University Press: Cambridge and New York, NY; 996 pp.

Tregoning P, Boers R, O'Brien D, Hendy M. 1998. Accuracy of absolute precipitable water vapor estimates from GPS observations. *J. Geophys. Res.* **103**: 701–710.

Vedel H, Huang XY, Haase J, Ge M, Calais E. 2004. Impact of GPS ZTD data on precipitation forecast in Mediterranean France and Spain. *Geophys. Res. Lett.* **31**: L02102.

Zwiers FW, Von Storch H. 2004. On the role of statistics in climate research. *Int. J. Climatol.* **24**: 665–680.